Bulletin of Volcanology (2019) 81: 23
https://doi.org/10.1007/s00445-019-1282-0

RESEARCH ARTICLE

# Mineralogy and chemistry of incrustations resulting from the 2014–2015 eruption of Fogo volcano, Cape Verde

Teresa P. Silva[1] · Daniel P. S. De Oliveira[1] · João P. Veiga[2] · Paula Ávila[3] · Carla Candeias[4,5] · Eduardo Salas-Colera[6,7] · Rita Caldeira[8]

Received: 27 July 2018 / Accepted: 22 February 2019 / Published online: 9 March 2019


## Abstract

The last eruption of the Fogo volcano, in the Cape Verde Archipelago, occurred in 2014–2015. A mineralogical and chemical study was undertaken on fumarole incrustations resulting from this event and compared with results obtained from the previous 1995 eruption. The mineralogical constitution of the fumarole deposits was assessed by X-ray diffraction and the chemical characterization was performed through X-ray fluorescence spectrometry with a wavelength dispersive system and by energy dispersive X-ray fluorescence at the European Synchrotron Radiation Facility. The most common compounds/minerals in solid deposits were sulfur, sodium chloride, and calcium sulphates with variable degrees of hydration, sodium sulphate, hydrated sulphates of sodium aluminum, potassium magnesium, or sodium magnesium and a fluorine-bearing mineral. Thenardite ($Na_2SO_4$) and its polymorph (phase III) were found simultaneously for the first time in incrustations, to the best of our knowledge. A large span of minor and trace elements present in incrustations (Na, Mg, Al, Si, P, S, Cl, K, Ca, Ti, V, Mn, Fe, Ni, Cu, Zn, As, Se, Br, Rb, Sr, Y, Zr, Nb, Mo, Ba, Ce, Tl, Pb) were also identified, some of them potentially hazardous to animal and human health. This study reveals that low temperature incrustations, allied to the atmospheric conditions of Fogo volcano, constitute a natural laboratory to observe the process of mineral formation—namely the $Na_2SO_4$ phase III considered metastable.

**Keywords** Fogo volcano · Cape Verde · Fumaroles · Incrustations · Volcanic gases · Minerals · Human and animal health

## Introduction

The process of mineral formation can be observed in fumaroles at active volcanoes, i.e., in a restricted space and time where the emanating hot gases are continuously depositing compounds/minerals. Gases released from the magma are rich in volatile components such as $H_2O$, $CO_2$, $SO_2$, $H_2S$, HCl, HF, $H_2$, $CH_4$, and CO, water vapor being the dominant constituent of high temperature (> 500 °C) volcanic gases (e.g., Symonds et al. 1994; Fischer 2008; Aiuppa 2015). Differences in the concentration distributions of these constituents are related to their fractionation during magma degassing and to their sources in magmas, the composition of volcanic gases being dependent on the temperature at fumaroles (Giggenbach 1996; Zelenski and Taran 2011). Recent studies on arc-volcanic gases have shown magmatic fluid uniformity in both

Editorial responsibility: T.P. Fischer

✉ Teresa P. Silva
teresa.pena@lneg.pt

[1] Mineral Resources and Geophysics Research Unit, National Laboratory for Energy and Geology (LNEG), Estrada da Portela, Apartado 7586, 2610-999 Amadora, Portugal

[2] CENIMAT/I3N, Departamento de Ciência dos Materiais, Faculdade de Ciências e Tecnologia, Universidade NOVA de Lisboa, 2829-516 Caparica, Portugal

[3] Mineral Science and Technology Unit, National Laboratory for Energy and Geology (LNEG), S. Mamede de Infesta, Portugal

[4] GeoBioTec - Geobiosciences, Geotechnologies and Geoengineering Research Center, Geosciences Department, University of Aveiro, Aveiro, Portugal

[5] EpiUnit - Epidemiology Research Unit, Environmental Health Department, Institute of Public Health, University of Porto, Porto, Portugal

[6] SpLine, Spanish CRG Beamline, European Synchrotron Radiation Facility (ESRF), Grenoble, France

[7] Instituto de Ciencia de Materiales de Madrid-CSIC, Madrid, Spain

[8] Geology, Hydrogeology and Coastal Geology Unit, National Laboratory for Energy and Geology (LNEG), Amadora, Portugal

the water isotopic composition and Cl content, as well as in the total composition (H–C–O–S–Cl–F), that contrast with volcanic fluids of non-arc volcanoes (De Moor et al. 2013; Paonita et al. 2013; Shinohara 2013; Taran and Zelenski 2015).

Volatile species transported by hot volcanic gases, either pure or resulting from their interaction with their hydrothermal surroundings, emitted through vents and fissures, are deposited or released to the atmosphere at the emitting source (Symonds et al. 1987). The material deposition formed by cooling and condensation or sublimation—fumarole incrustations—generates a colored field and constitutes an indication of the role played by magmatic fluids in the processes of mineral formation (e.g., Lacroix 1907; Stoiber and Rose 1974; Óskarsson 1981, 1984; Toutain et al. 1990). These studies have all shown that incrustations retain a significant amount of the transported components that are carried in the minerals as nanometer-sized inclusions. For example, the 1902 eruption of Santa Maria, Guatemala, was one of the largest volcanic eruptions of the twentieth century (Williams and Self 1983). New eruptions began in 1922 (Rose 1973), and studies performed between 1964 and 1969 on condensates from Central American volcanoes (including the dome that began to grown within the Santa Maria caldera: Santiaguito) showed that condensate chemistry depended on fumarole location and time of collection relative to the eruptive and cooling history of the emplacement event (Stoiber and Rose 1970). The most abundant and frequently found minerals in incrustations were sulfur, hematite, halite, sylvite, gypsum, ralstonite, anhydrite, thenardite, and langbeinite (Stoiber and Rose 1974). Other examples could be cited: sulfur, opaline silica, gypsum, ralstonite, and thenardite at Hawaiian volcanoes (Naughton et al. 1976); gypsum, anhydrite, sulfur, tridymite, halite, and soda alum at Mount St. Augustine, Alaska (Kodosky and Keskinen 1990); and the extensive work of fumarolic minerals at European volcanoes completed by Balić-Žunić et al. (2016). The description of fumarole products resulting from low-temperature volcanic emissions, including iron, magnesium, aluminum, and manganese chlorides (Pelloux 1927) as well as sulfur and realgar at Vesuvius, have also been recorded. Yellow amorphous iron chloride, cristobalite, and minor amounts of ralstonite (60–80 °C), soda-alum (150 °C)—or even anhydrite and sodium aluminum sulphate (350 °C) in one fumarole of Santiaguito volcano (Stoiber and Rose 1969) have also been noted. Sulfur, gypsum, alunogen, and other hydrous sulphates in European fumarolic systems are well-documented by Balić-Žunić et al. (2016).

Studies have also been completed on incrustations left at systems active in the Atlantic Ocean, including Iceland, Azores, Canary Islands, Tristan da Cunha, and on the island of Fogo in the Cape Verde Archipelago (e.g., Baker et al. 1964; Figueiredo et al. 1997; Jakobsson et al. 2008; Melián et al. 2012; Carvalho et al. 2014). In each case, the incrustations provide indirect sources of information on the nature of volcanic degassing and, particularly, on heavy metal transport by lava degassing (Toutain et al. 1990). A detailed knowledge of the nature and range of heavy elements carried by gases emanating from fumaroles following a volcanic eruption, or during periods of unrest, is vital in the domains of environment, geochemistry, and volcano risk assessment (e.g., Chiodini et al. 1995, 2002; Africano et al. 2002; Orlando et al. 2011). Frequently, elements such as Hg, Pb (Ferrara et al. 1995), and the highly poisonous element Tl are present, and pose a significant threat to human (and environmental) health (Rodríguez-Mercado and Altamirano-Lozano 2013). This feature was noticed following the 1995 eruption of Fogo volcano and was studied by synchrotron X-ray microprobe (Figueiredo et al. 1999). In spite of this finding, little information exists about the mineralogy and chemistry related to fumarole deposits, and about the chemical composition of gases emitted, by Fogo and, in particular, during the last two eruptive periods (1995 and 2014–2015).

To contribute to a better knowledge on the process of mineral formation at low temperature (< 250 °C), we here present a mineralogical study performed on incrustations (materials formed by cooling and condensation or sublimation and deposited in the field around fumaroles) from the latest eruption of Fogo volcano. The occurrence of thenardite ($Na_2SO_4$) and its polymorph (phase III) in one single locality represents, to the best of our knowledge, the first discovery of both of these phases occurring simultaneously. We discuss this particular observation in terms of transition temperatures and phase stabilities. Finally, the comparison with minerals resulting from the previous eruption (1995) is undertaken. Moreover, the chemical study based on these materials is used to infer the volcanic gas' composition in terms of their heavy metal contents and toxicity.

## Geological setting

Fogo Island, part of the Cape Verde Archipelago (Fig. 1), is the only island in the archipelago with known historic volcanic activity, since the discovery of the archipelago in the fifteenth century as registered in logs of ships (Ribeiro 1998). The island was formed in an oceanic environment by a mantle plume—hot-spot type mechanism (Mata et al. 2017). Volcanism is essentially alkaline and it is assumed that Fogo is currently located above a hot-spot (Torres et al. 1995, 1997; Silva et al. 1997).

Fogo Island is nearly circular in shape approximately 25 km in diameter with a maximum altitude of 2829 m a.s.l., corresponding to a central volcano with its center offset to the NE to a lateral east flank collapse (Day et al. 1999; Maccaferri et al. 2017). Fogo also has more than 100 adventive cones, 50 to 100 m high, distributed across the flanks of the main eruptive cone and summit caldera—Chã das Caldeiras. This

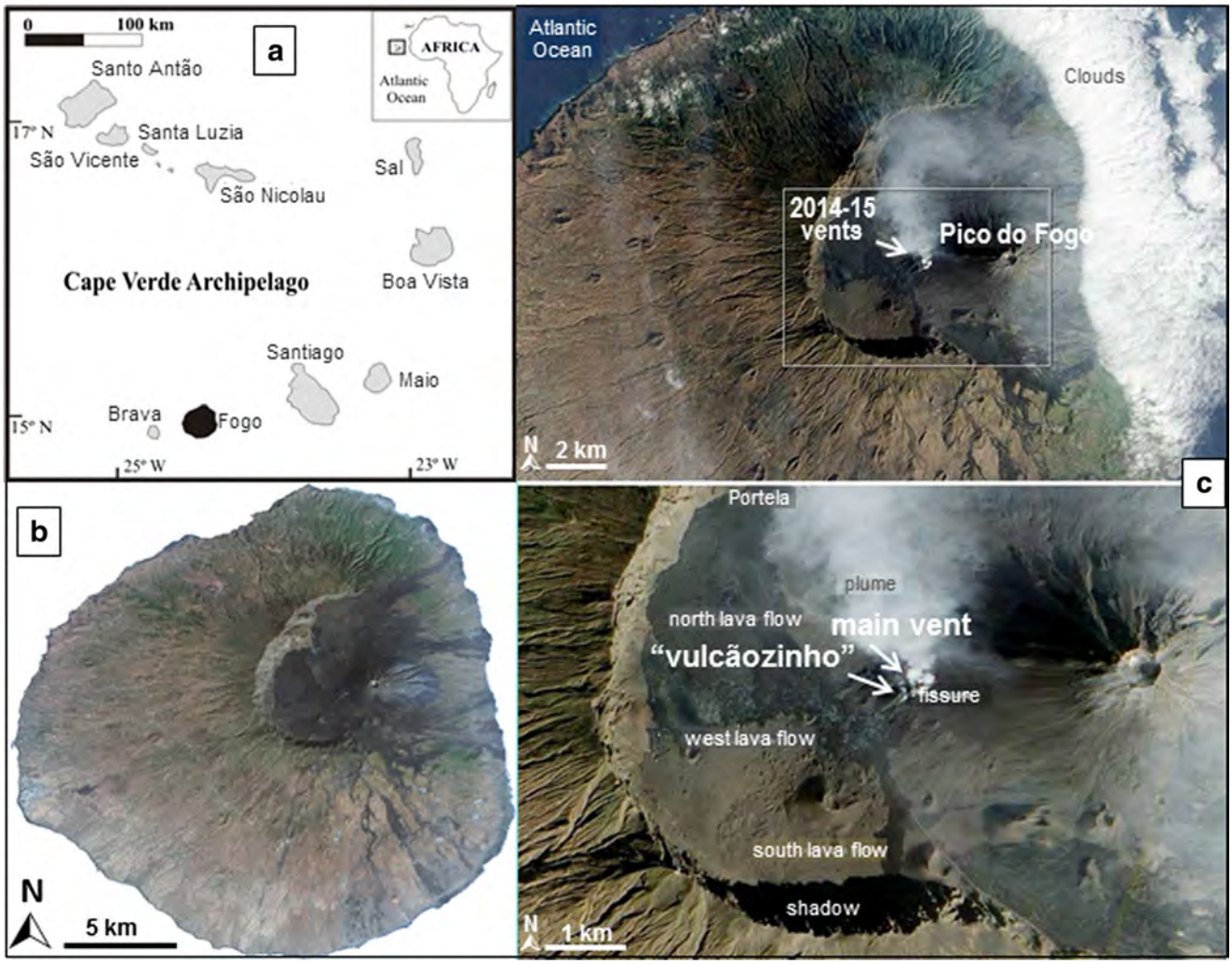


**Fig. 1** **a** Map of the Cape Verde Archipelago. Satellite images of Fogo Island. **b** From Sentinel 2 captured on 6 February 2017 (true color RGB composite). **c** Sampling sites, adapted from Global Volcanism Program 2017 (image captured on 24 December 2014)

caldera is approximately 9 km in N-S diameter, and whose steep back wall—Bordeira—reaches 1 km in height. Within this caldera, the 1100-m-high cone of the Pico do Fogo volcano (currently the highest point on the island), with a crater 100 to 200 m deep and 500 m in diameter was built; its first activity is unknown, but after the second half of the eighteenth century, the eruptive occurrences begun at the adventive cones (Torres et al. 1997; Ribeiro 1998).

The most recent eruptive events occurred in 1995 and 2014–2015, both of which produced extensive lava flow fields (a'a and pahoehoe) at Chã das Caldeiras, which destroyed houses and agricultural land (Jenkins et al. 2017). The local population was about 1200 inhabitants in 2014, and the economy was based on agriculture (mainly vine and fruit plantations), grazing, and tourism (Vieira et al. 2017). The latest eruption (November 23, 2014 to February 7, 2015) occurred on a NE-SW trending 700-m-long fissure located on the SE flank of the previous 1995 cinder cone, an adventive vent developed on the SW flank of the younger Pico do Fogo volcano (Fig. 2). The 2014–2015 eruption was more explosive than the one in 1995, varying from Hawaiian to Strombolian and Vulcanian activity phases, which sometimes occurred simultaneously at the different aligned craters. Lava flow simulations have been carried out to better understand the 2014–2015 lava flow crisis and to prepare for the next inevitable eruption (Richter et al. 2016).

## Experimental

### Sampling

Two sampling campaigns were carried out (Table 1 and Fig. 1). In November 2016, we collected rocks (basaltic lava) and incrustations deposited on rocks from near the 2014–2015 main vent (Figs. 3 and 4), while in February 2017 we recorded

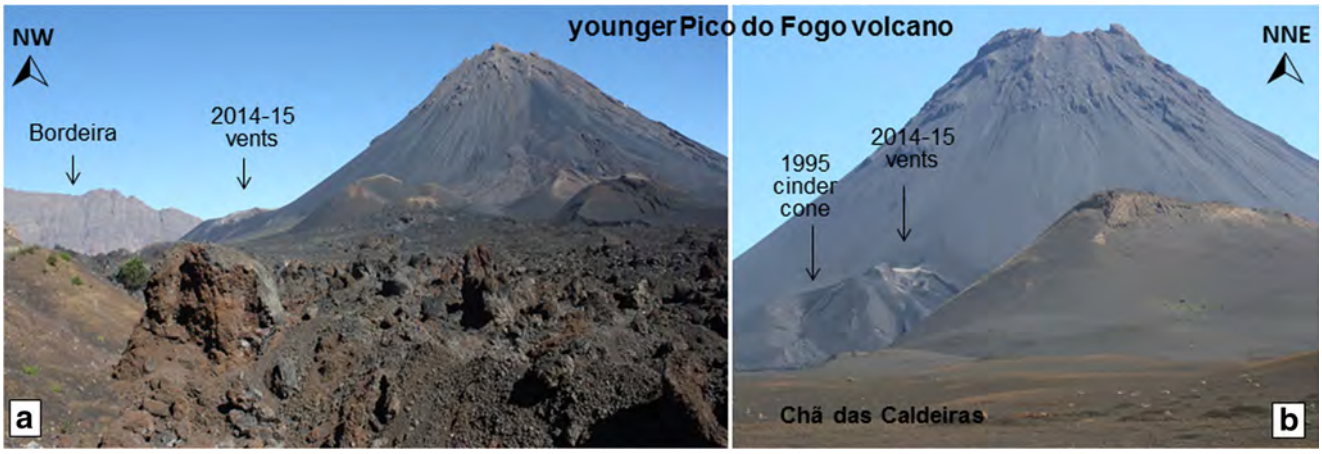


**Fig. 2** Younger Pico do Fogo volcano (principal eruptive cone) is the highest point on Fogo Island (Cape Verde) inside the Chã das Caldeiras (around 1100 m high): **a** view of the steep rock wall (Bordeira) that reaches 1 km in height. **b** Location of the last two eruptive events (the 2014–2015 eruption occurred on the flank of the previously formed 1995 cinder cone), viewed at a distance of about 1500 m across the Chã das Caldeiras

the temperatures in the area around the samples with a digital thermometer using a thermocouple type "K"—Chromel-Alumel (Metra Instruments, http://www.metra-instruments.com/PDF/6504.pdf).

Adjacent to the main vent (Fig. 3), the fumaroles were almost imperceptible in both field campaigns. Yellow—sulfur—(Fig. 5a) and white precipitates/sublimates were deposited in the field as well as orange-red altered rocks. White incrustations were collected along the walls of a higher-temperature unstable fracture (Fig. 5b). The highest registered temperature (238 °C) was measured in a hole (Fig. 5c) containing white material (collected near the surface), in alignment with the fracture and probably connected to it.

**Table 1** Brief description of samples collected during two campaigns on Fogo volcano and measured temperature close to the sample

| Sampling campaign | Location | Sample reference | Description | Temperature (°C) |
|---|---|---|---|---|
| November 2016 | Surroundings of the main vent (rocks with colored incrustations deposited on the field) | S2 | Reddish rock with white opaque crystals | |
| | | S3 | Rock with hyaline sulfur | |
| | | S4 | Aggregate with yellow and orange sulfur plus white incrustations | |
| | | S5 | Reddish/brownish rock with white opaque incrustations | |
| | | S6 | Whitish rock and pink | |
| February 2017 | | F8/17 | Rock with hyaline sulfur, white crystals and whitish hyaline powder | |
| | | F9/17 | Sulfur aggregates and white incrustations | 162 |
| | | F10/17 | Reddish incrustation in the rock | |
| | | F11/17 | Rock with sulfur (aggregate and hyaline) and white incrustations | |
| | | F12/17 | White and yellow powders in the rock | |
| | | F13/17 | Greenish sulfur | |
| | | F14/17 | Reddish rock with white incrustations | |
| | | F17/17 | White aggregate on the field | 76 |
| | | F25/17 | White (hygroscopic) and yellowish incrustations | |
| | | F26/17 | White powder (dry) | |
| | | F27/17 | Yellow and brown-orange incrustations | |
| | Walls of an unstable fracture, near the main vent | F18/17 | White powder | 182 |
| | Walls of a pit, near the main vent | F19/17 | White powder | 238 |
| | "Vulcãozinho" (smaller vent) | F24/17 | White powder | |


**Fig. 3** Main vent of 2014–2015 eruption on Fogo Island (distance around 3 km between main vent and Bordeira) and lava flow field at Chã das Caldeiras

There is a second, smaller vent, called by the local population "vulcãozinho" (little volcano), located at lower altitude than the main one (Figs. 1, 6, and 7). It has a pit created by the eruption in which white incrustations were found deposited on the rocks. A big tunnel, which also contains white incrustations, enters the bottom of the pit, from which lava came out at the beginning of the eruption, before being swallowed by the pit.

## Methods and techniques

A Philips PW 1500 powder diffractometer with Bragg-Brentano geometry, equipped with a large-anode copper tube operating at 50 kV–40 mA and a curved graphite crystal monochromator, was used to collect X-ray diffraction (XRD) patterns of the powdered samples previously observed using a stereomicroscope (Zeiss, Stemi SV-11). The images were collected with a digital Zeiss camera (Axio-Cam Mrc). An effort was made to select pure phases of incrustations with respect to the morphology and color, avoiding contamination by minute lava fragments. The thermodynamic conditions which prevail during the deposition of minerals from volcanic gases favor the formation of predominantly fine-grained, dispersed, cryptocrystalline, and, in some exceptional cases, imperfect crystalline aggregates (Vergasova and Filatov 2016). The identification of fumarole minerals was in some cases difficult due to the presence of a mixture of phases and uncommon mineral associations.

For this reason, a semi-quantitative chemical analysis through X-ray fluorescence spectrometry with wavelength dispersive system (XRF-WDS) was performed. For the elemental analysis, a PANalytical AXIOS sequential spectrometer (Rh X-ray tube, 4 kW) under He flow was used. Samples were analyzed in powder form to avoid chemical heterogeneities and crystalline effects. Standardless semi-quantitative analysis was performed with the SuperQ IQ+ software package (Figueiredo et al. 2018).

As a preliminary approach, the chemical composition of four incrustation samples was also obtained by energy dispersive X-ray fluorescence (EDXRF) at the European Synchrotron Radiation Facility (ESRF) in Grenoble/France. The experiments were performed with

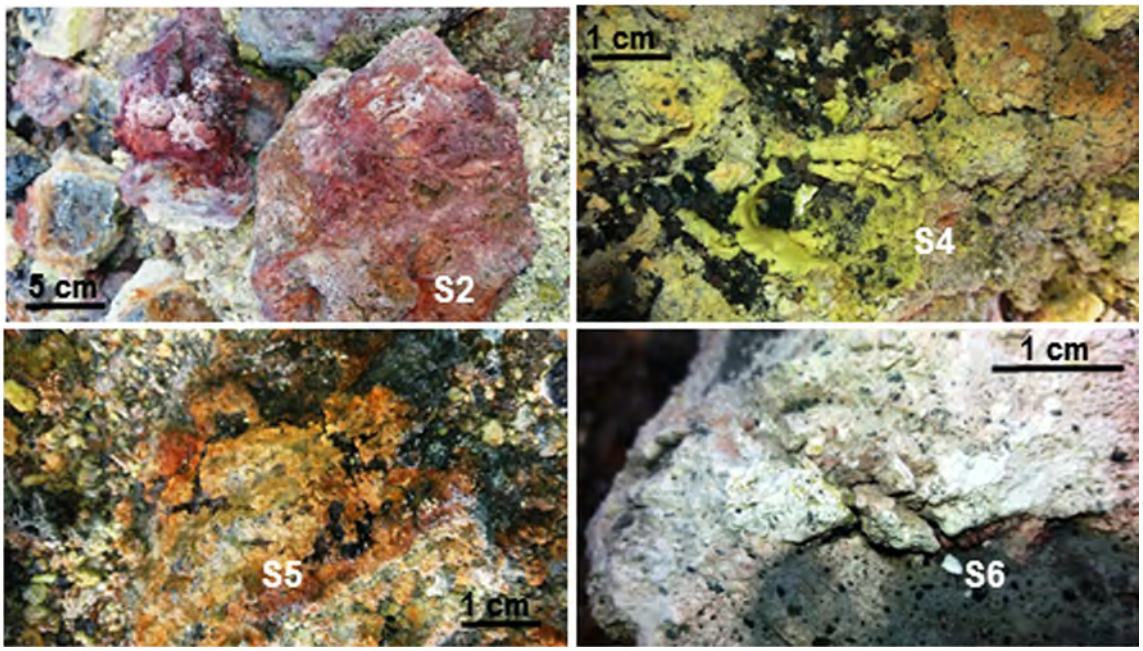


**Fig. 4** Samples of rocks (basaltic lava) and incrustations collected in November 2016, from near the 2014–2015 main vent (see Table 1 for description)

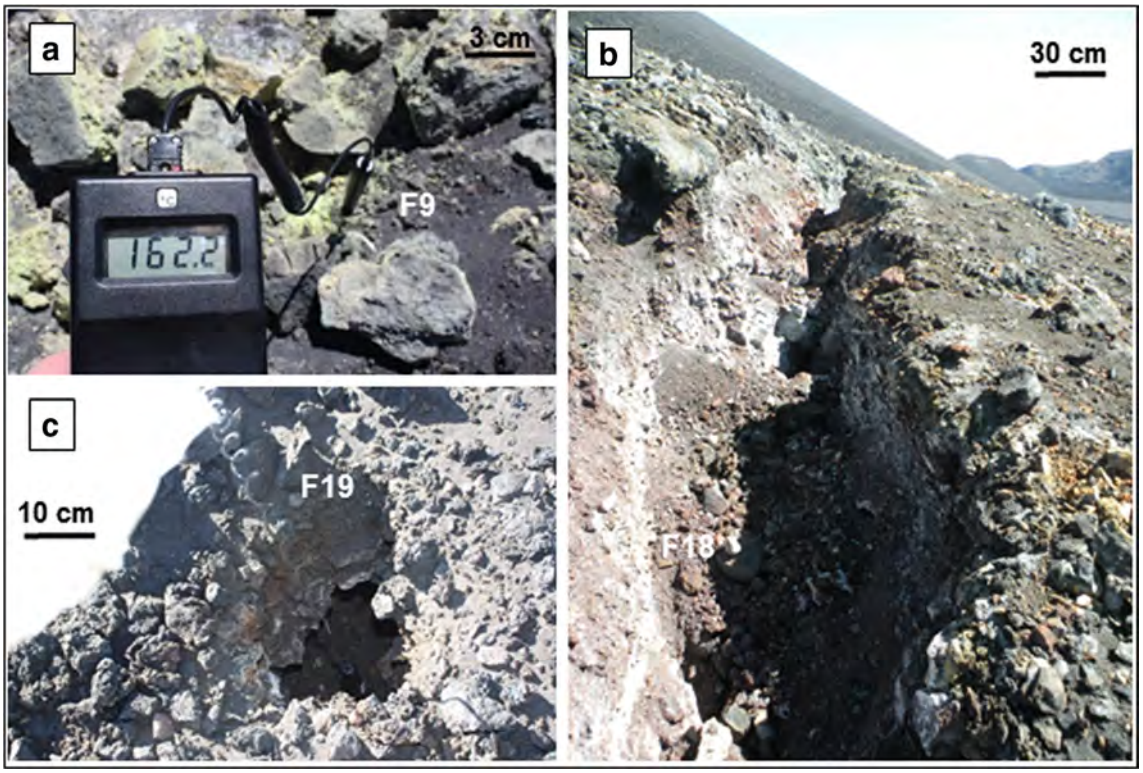


**Fig. 5** February 2017 sampling campaign. **a** Sulfur (F9, yellow) close to the main vent and the registered temperature near the sample. **b** Unstable fracture where white incrustations (F18, 182 °C) were collected along the walls. **c** The highest temperature (238 °C) was measured at the bottom of a pit lined containing white material (F19)

the instrumental set up of beamline BM 25A, using an excitation energy of 29.58 keV (powdered samples were placed between two Kapton foils, a special pure adhesive tape that reduces interference from any support material) and an irradiated area of 1 $mm^2$. A Sirius Si (Li) 13-element fluorescence detector was employed for EDXRF experiment. Si (Li) crystals have a good spectral response over an energy range between 2 and 30 keV. The high brilliance of synchrotron X-rays allows for remarkably low limits of detection for most chemical elements, thus enabling the analysis of trace and sub-trace species hosted by a mineral (provided


**Fig. 6** Image of the smaller vent, called "vulcãozinho" (little volcano) by the local population, located at a lower altitude than the principal vent. The circle marks a person for scale near the main vent


**Fig. 7** White incrustations (F24) surrounding "vulcãozinho." View of a pit with a big tunnel crossing it, also containing white material

the medium atomic number of the major components is relatively low). The energy dispersive spectra collected over a period of 300 s for each sample were fitted using the PyMca software (Solé et al. 2007).

## Results

### Mineralogical characterization

The mineralogical composition of the incrustations was obtained by XRD (Table 2), after careful selection using a stereomicroscope (illustrative images can be observed in Fig. 8). However, some phases such as olivine, pyroxene, and titanite are attributed to basaltic lava. More than one phase was identified for the majority of samples, with the first one being the most representative for each sample assigned in Table 2.

Out of interest, sample F20/17 is a whitish powder that the local population usually uses to treat certain diseases (called "scontra"), and it is also sold to tourists. XRD analysis of this sample showed the presence of a mixture of anhydrite ($CaSO_4$) and gypsum ($CaSO_4.2H_2O$) with vestigial sulfur.

The main phases identified in the incrustations were sulfur (common orthorhombic form, α-S), sodium chloride (halite, NaCl), calcium sulphates with variable degrees of hydration (anhydrite, $CaSO_4$, bassanite, $CaSO_4.1/2H_2O$, and gypsum, $CaSO_4.2H_2O$), anhydrous sodium sulphate (thenardite and $Na_2SO_4$ (III)) (Fig. 9), sodium aluminum sulphate hydrate (tamarugite, NaAl $(SO_4)_2.6H_2O$), potassium magnesium sulphate hydrate (picromerite, $K_2Mg(SO_4)_2.6H_2O$), sodium magnesium sulphate hydrate (bloedite, $Na_2Mg(SO_4)_2.4H_2O$), or with more metallic elements (bianchite, $(Zn_{0.69}Fe_{0.21}Mg_{0.10})SO_4.6H_2O$) and a fluoride (ralstonite, $Na_xMg_xAl_{1-x}(F,OH)_3.(H_2O)n$).

### Chemical analysis

The semi-quantitative results obtained by XRF-WDS for selected powder samples (Table 3) are in accordance with the main mineralogical phases identified. Sulfur samples are quite pure. The highest Mg contents belong to samples of bloedite and picromerite (9%) and bianchite (7%). The K contents of between 18 and 27% correspond to picromerite, and of around 10% to ralstonite. As expected, the higher levels of Ca and Sr belong to incrustations with anhydrite, bassanite, and gypsum. Samples of altered rock (basaltic lava) are rich in the heavy elements Zr, Ba, Ce, Tl, as well as Ti and Fe (F12-powder scraped off the rock, F14-red rock, and F27-yellow and orange incrustations).

The comparison of EDXRF spectra (Fig. 10) shows that Se is carried by massive S, and As is present in four samples, with the highest values being in the anhydrite and gypsum mixtures (F20-white incrustations, aggregate, and disaggregate). Br is present in the halite sample (F19). In addition, low concentrations (traces) of the following elements can be detected: Pb, Rb, Sr, Y, Zr, Nb, and Mo, especially in F20 samples (the intensity of the lines close to the excitation energy is increased). The presence of lithophile elements like Rb, Sr, Y, Zr, and Nb is possibly due to minor silicate phases. The low detection limits also make it possible to identify Cu and Zn.

**Table 2** XRD mineralogical characterization of incrustations from 2014 to 2015 eruption of Fogo volcano, Cape Verde (JCPDF card quoted bellow)

| Location | Sample reference | Description | Main identified phases |
|---|---|---|---|
| Main vent (field) | S2 | Reddish rock | Amorphous |
| | S3 | Rock with hyaline sulfur | S + Pi |
| | S4 | Yellow sulfur | S |
| | | Orange sulfur | S |
| | | White incrustation and sulfur | A + S + G |
| | S5 | Reddish rock with white opaque crystals | Pi + A |
| | | Brownish rock with white powder | Pi + G |
| | S6 | White and pink rock fragments | Amorphous + Pi |
| | F8/17 | White crystals | A + Ba |
| | | Whitish hyaline powder | G + A |
| | F9/17 | Sulfur aggregate | S |
| | | White incrustations | Ta + B |
| | F10/17 | Reddish incrustation | A + Ba + S |
| | F11/17 | Sulfur aggregate | S |
| | | Hyaline sulfur | S |
| | | White powder | A + Ba + S (vtg) |
| | | White aggregate | Ba + A (vtg) + Pi? (vtg) |
| | F12/17 | Powder scraped from the rock | Amorphous + G + A + S (vtg) |
| | | Gypsum crystals? | G + A |
| | | Sulfur aggregate | S + G (vtg) |
| | | Hyaline sulfur | S + G (vtg) |
| | F13/17 | Greenish sulfur | S + O (vtg) |
| | F14/17 | Reddish rock | Ti + R |
| | | White incrustations | Bl + T + P + H + S (vtg) |
| | F17/17 | White aggregate | Ta + B |
| | F25/17 | White incrustations (hygroscopic) | T + Bl + H? |
| | | Yellowish incrustations | T + Bl + P + H + S (vtg) |
| | F26/17 | White powder (dry) | T + Bl + H + P + S (vtg) |
| | F27/17 | Yellow incrustations | Ti + R (vtg) |
| | | Brown-orange incrustations | R |
| Main vent (fracture) | F18/17 | White powder | A + Ba + S (vtg) |
| | | Sub-rounded white crystals | Ba + A + G? (vtg) |
| | | White opaque crystals | Amorphous + Ti? |
| Main vent (pit) | F19/17 | White powder | H + T + SS |
| "Vulcãozinho" (smaller vent) | F24/17 | White powder | T + H |
| Unknown | F20/17 | White aggregate | A + G |
| | | White powder (disaggregate) | G + A + S (vtg) |

A—anhydrite, $CaSO_4$ (#37-1496); B—bianchite, $(Zn_{0.69}Fe_{0.21}Mg_{0.10})SO_4.6H_2O$ (#12-16); Ba—calcium sulphate hydrate (Bassanite), $Ca_2(SO_4)_2.H_2O$ (#41-224); Bl—bloedite, $Na_2Mg(SO_4)_2.4H_2O$ (#88-1789); G—gypsum, $CaSO_4.2H_2O$ (#6-0046); H—halite, NaCl (#5-0628); O—olivine–Fayalite, $Fe_2SiO_4$ (#20-1139); P—picromerite, $K_2Mg(SO_4)_2.6H_2O$ (#21-1400); Pi—pyroxene–Diopside, $CaMg\ (SiO_3)_2$ (#71-1067); R—ralstonite, $Na_{0.88}Mg_{0.88}Al_{1.12}(F,OH)_6.H_2O$ (#18-1085); S—sulfur, S orthorhombic (#8-247); SS—sodium sulphate (Form III), $Na_2SO_4$ (#24-1132); T—thenardite, $Na_2SO_4$ (#37-1465); Ta—tamarugite, $NaAl\ (SO_4)_2.6H_2O$ (#71-2385); Ti—titanite, $CaTiSiO_5$ (#25–177); vtg—vestigial content

A large span of minor and trace elements was identified by combining both techniques (Na, Mg, Al, Si, P, S, Cl, K, Ca, Ti, V, Mn, Fe, Ni, Cu, Zn, As, Se, Br, Rb, Sr, Y, Zr, Nb, Mo, Ba, Ce, Tl, Pb), which were present in incrustations deriving from the condensation and sublimation of volcanic gases (though it cannot be excluded that some elements might result from lava impurities).

## Discussion

### Low-temperature incrustations

Incrustations can be grouped according to the mineralogy in terms of elemental sulfur, sulphates, and halides. The species

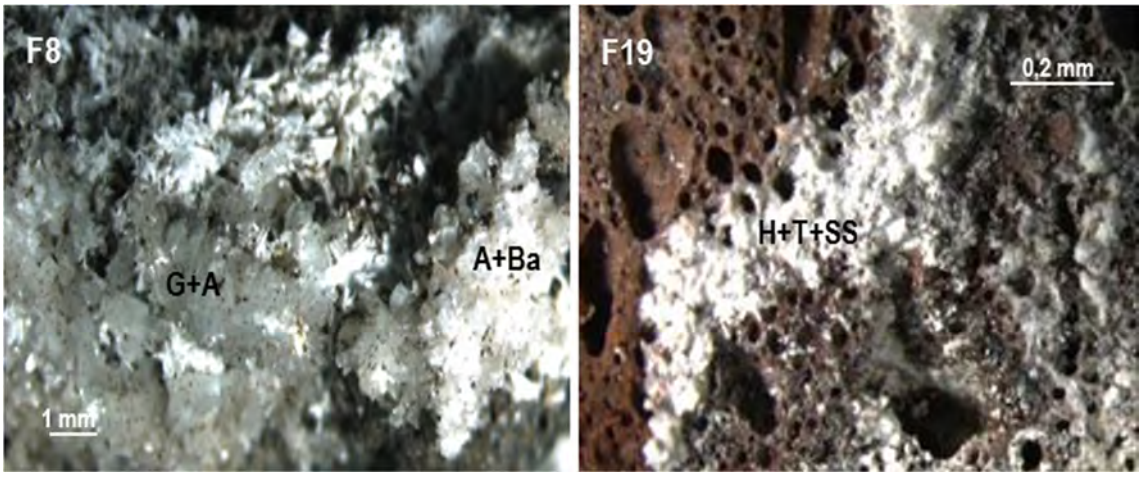


**Fig. 8** Stereomicroscope images of some studied samples with the corresponding mineralogical phases assigned: F8-white crystals (A–Anhydrite + Ba–Bassanite); F8-whitish hyaline material (G–Gypsum + A–Anhydrite); F19-white material (H–Halite + T–Thenardite + SS–Sodium sulphate, form III)

distribution around the main vent (Tables 1 and 2) shows that sulfur was dominant, but anhydrite, bassanite, gypsum, thenardite, bloedite, tamarugite, picromerite, ralstonite, and halite were also found at about 70 °C and about 160 °C. There was also crystallized anhydrite and bassanite on the walls of one E-W fracture (182 °C) located around 20 m from the main vent (see Figs. 2b and 5b). Halite and thenardite, and its polymorph (phase III), were identified inside a pit (238 °C) located near to the 1995 cinder cone, around 80 m away from the main vent (Fig. 2b). At a smaller vent located at lower altitude (Fig. 6), only thenardite and halite were found.

Sulfur was present as an orthorhombic mineral in the form of yellow hyaline crystals and massive aggregates. The common, stable sulfur (α-S), which is very frequent in volcanic areas, is constituted of $S_8$ molecules. Due to the molecular character of the chemical bonding in native sulfur, the uptake of other elements during crystallization is extremely selective, with only Se and possibly As being capable of being retained in solid solution (Figueiredo et al. 1999).

Sulphate phases are dominated by common anhydrite (β-$CaSO_4$), bassanite, and gypsum. Anhydrite is associated with bassanite, hemihydrate (e.g., sample F18/17, $T = 182$ °C), or with gypsum. The metastable polymorph γ-$CaSO_4$ (soluble anhydrite) obtained by slow dehydration of gypsum or hemihydrate at 100 °C is hexagonal and its transformation to anhydrite begins at 150 °C (Flörke 1952). In natural samples, it is known that gypsum coexists with anhydrite along with minor amounts of alkali and alkaline halide impurities and that the equilibrium temperature of the gypsum-anhydrite phase is lowered due to the presence of impurities that prevent the free movement of water molecules. The transition of gypsum to bassanite is associated with a rearrangement of sulphate ions,

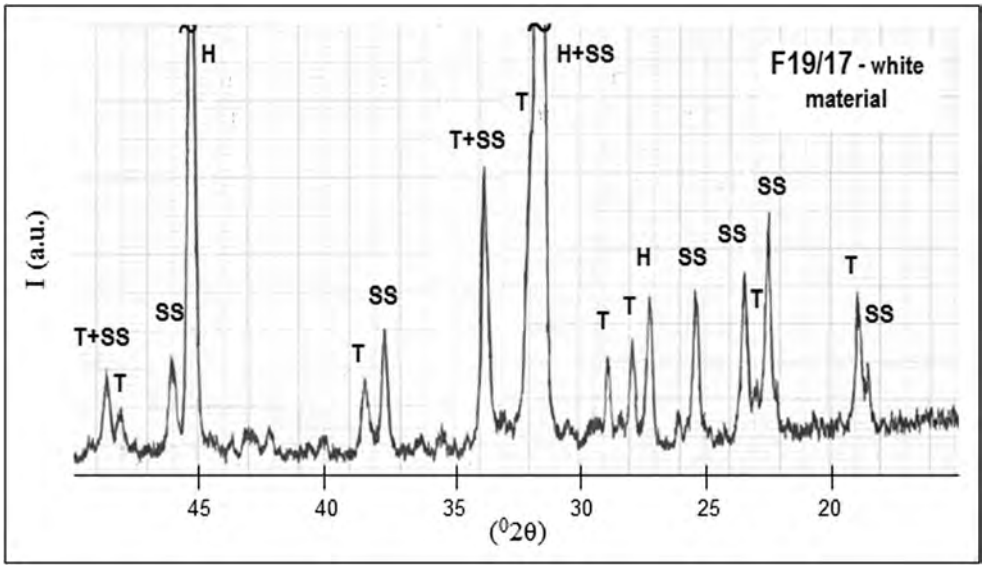


**Fig. 9** XRD pattern collected from white material of sample F19/17. Assigned phases in decreasing percentage: *H* halite (NaCl); *T* thenardite ($Na_2SO_4$); *SS* (sodium sulphate, form III)

**Table 3** Semi-quantitative normalized chemical analysis (wt%) obtained by XRF-WDS, of incrustations and altered rock from 2014 to 2015 eruption of Fogo volcano, Cape Verde

| | F8 | F9 | | F11 | | | F12 | | | | F13 | F14 | | F17 |
|---|---|---|---|---|---|---|---|---|---|---|---|---|---|---|
| | Whit. hyal. powd. | S aggr. | White incrus. | S aggr. | White powd. | White aggr. | Powd. from rock | Gyp? | S aggr. | S hyal. | S green | Red rock | White incrus. | White aggr. |
| Na | | | 8.9 | | | | | | | | | 2.8 | 18.1 | 5.1 |
| Mg | | | 4.2 | 0.1 | 0.7 | | 0.6 | | | | 0.3 | 4.5 | 8.9 | 6.7 |
| Al | 1.3 | | 15.6 | 0.1 | 1.3 | 1.2 | 2.0 | 0.3 | 0.2 | 0.4 | 0.6 | 15.2 | 1.2 | 15.5 |
| Si | 5.5 | | 2.8 | 0.2 | 3.5 | 9.0 | 52.9 | 6.3 | 1.5 | 0.5 | 6.1 | 31.9 | 0.7 | 1.5 |
| P | | | | | | | 0.8 | | | | | 0.7 | | |
| S | 34.9 | 100.0 | 59.9 | 99.6 | 36.4 | 29.7 | 17.6 | 32.2 | 94.4 | 97.8 | 89.9 | 0.9 | 49.8 | 66.2 |
| Cl | | | | | | | | | | | 0.9 | 1.7 | 0.9 | |
| K | 0.8 | | 2.8 | | 1.0 | 1.3 | 1.4 | 0.2 | 0.1 | | 0.3 | 4.5 | 17.9 | 1.5 |
| Ca | 56.3 | | 2.9 | | 53.7 | 51.5 | 7.5 | 59.1 | 3.7 | 1.3 | 0.7 | 13.6 | 0.9 | 0.9 |
| Ti | | | 0.4 | | 0.5 | 1.6 | 9.4 | 0.9 | 0.1 | | 0.6 | 5.3 | 0.3 | 0.3 |
| V | | | | | | | | | | | | 0.2 | | |
| Mn | | | 0.4 | | | | 0.1 | | | | | 0.3 | 1.0 | 0.9 |
| Fe | 1.3 | | 1.9 | | 2.8 | 5.4 | 7.1 | 0.8 | | | 0.5 | 18.1 | 0.4 | 1.3 |
| Ni | | | | | | | | | | | | 0.1 | | |
| Zn | | | | | | | | | | | | | | 0.1 |
| Se | | | | | | | | | | | | | | |
| Sr | | | | | 0.1 | 0.2 | | 0.3 | | | | | | |
| Zr | | | | | | | 0.1 | | | | | | | |
| Ba | | | | | | | 0.2 | | | | | | | |
| Ce | | | | | | | 0.3 | | | | | | | |
| Tl | | | | | | | | | | | | | | |

| | F18 | | | F19 | F20 | | F24 | F25 | | F26 | F27 | |
|---|---|---|---|---|---|---|---|---|---|---|---|---|
| | White powd. | Round white cryst. | White opaq. Cryst. | White powd. | White aggr. | White powd. Disag. | White powd. | White incrus. Hygr. | Yell. incrus. | White powd. (dry) | Yell. incrus. | Oran. incrus. |
| Na | | | | 32.8 | | | 34.3 | 25.2 | 15.6 | 26.4 | 1.1 | 9.5 |
| Mg | 0.7 | 0.5 | 1.0 | | | 0.4 | 0.2 | 4.8 | 4.9 | 3.8 | 1.9 | 3.1 |
| Al | 2.2 | 1.6 | 4.7 | 1.0 | 0.1 | 1.7 | 0.3 | 0.3 | 0.4 | 0.3 | 5.2 | 25.4 |
| Si | 3.4 | 5.0 | 79.1 | 1.2 | 4.1 | 26.5 | 0.3 | 0.2 | 0.3 | | 60.3 | 2.8 |
| P | | | | | | | | | 1.9 | | | |
| S | 28.5 | 31.0 | 5.2 | 20.5 | 33.5 | 34.8 | 41.9 | 43.0 | 40.8 | 42.1 | 0.4 | 0.5 |
| Cl | 0.8 | | 1.3 | 39.5 | | 0.3 | 17.9 | 5.0 | 4.2 | 5.8 | 9.0 | 2.9 |
| K | 1.0 | 0.8 | 0.6 | 2.5 | 0.1 | 0.4 | 4.0 | 19.8 | 27.2 | 20.7 | 1.4 | 10.3 |
| Ca | 58.5 | 55.4 | 2.6 | 2.0 | 56.5 | 26.7 | 0.7 | 0.6 | 3.0 | 0.3 | 7.4 | 23.5 |
| Ti | 1.0 | 1.3 | 4.0 | | 5.0 | 7.7 | 0.1 | | | | 7.9 | 3.0 |
| V | | | | | | | | | | | | 0.1 |
| Mn | | | | | | | | 0.9 | 1.2 | 0.5 | 0.2 | 0.6 |
| Fe | 3.5 | 3.6 | 1.4 | 0.6 | | 1.4 | 0.1 | 0.1 | 0.5 | | 5.1 | 17.5 |
| Ni | | | | | | | | | 0.1 | | | |
| Zn | | | | | | | | | | | | |
| Se | | | | | | | | | | | | 0.1 |
| Sr | 0.5 | 0.8 | | | 0.6 | 0.1 | | | | | | 0.3 |
| Zr | | | | | | | | | | | | 0.1 |
| Ba | | | | | | | | | | | | |
| Ce | | | | | | | | | | | | |
| Tl | | | | | | | | | | | | 0.2 |

*aggreg* aggregate, *cryst* crystals, *disag* disaggregate, *gyp* gypsum, *hyal* hyaline, *hyg* hygroscopic, *incrus* incrustations, *opaq* opaque, *oran* orange, *powd* powder, *whit* whitish, *yell* yellow

Sample reference and description are simplified

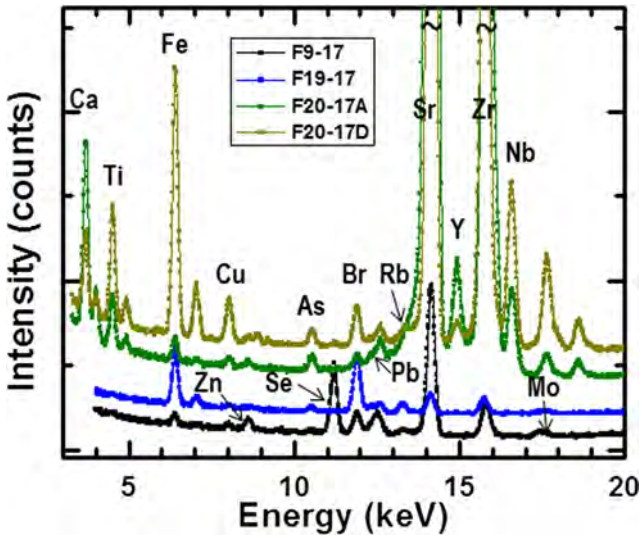


**Fig. 10** Energy dispersive X-ray fluorescence (EDXRF) spectra (excitation energy of 29.58 keV) collected for samples F9/17 (sulfur aggregate), F19/17 (white material), F20/17A, and D (white material aggregate and disaggregate, respectively). Only the diagnostic line of each element is assigned

but such changes are marginal during the transition of bassanite to anhydrite (Prasad et al. 1998). Sodium chloride solutions promote a step-wise dehydration process and a decrease in the temperature of gypsum-bassanite-anhydrite transformation (Hardie 1967; Prasad et al. 1998). However, halite was not found associated with calcium sulphate minerals in Fogo volcano. Bassanite occurrence in fumaroles is not as common as anhydrite or gypsum, but has also been referenced (Balić-Žunić et al. 2016).

Tamarugite was only found at the main vent as a white material (e.g., sample F17/17, $T = 76.5$ °C) with bianchite. This mineral has been described as occurring at Vulcano, Italy (Lombardi and Sposato 1981) and at Te Kopia, New Zealand (Mackenzie et al. 1995). Bloedite and picromerite were found together at the main vent, associated with thenardite and halite. Of the minerals identified, thenardite occurs in a particular situation and is thus treated in a separate section.

The presence of Cl was found only in halite, which occurred in a pit with the highest temperature registered (238 °C) at the main vent (sample F19/17), and also at the smaller vent "vulcãozinho" (sample F24/17). In both cases, halite was associated with thenardite unlike what was noticed in previous eruption (Silva 1999).

The observed mineral associations are spatially confined to different zones in the field, and provide evidence of the distinctive features of the gas compositions that arrive at the surface (gases of the S, Cl, and F group, and water vapor). The interaction between fluorine-bearing gases and volcanic rocks gives rise to a more or less superficial discoloration of the pyroclastic material and the formation of ralstonite (brownish in color). This mineral was found for the first time in Ivigtut (Greenland) and described by Brush in 1871 (Palache et al. 1951). Ralstonite has frequently been observed in other fumarole incrustations: for instance, Rosenberg (1988) mentions the existence of three hydrated aluminum fluorides in incrustations from Mount Erebus (Antarctica), including ralstonite. Rosenberg also notes that F-rich volcanic gases are associated with alkaline volcanoes, as is the case of Fogo volcano. Ralstonite was identified in this study (e.g., sample F27/17) and in the previous eruption (1995) incorporating an orange gel (Figueiredo 1997). Although fluorine was not chemically detected, since it is a very light element, its presence is clearly indicated by ralstonite, indicating that HF is a possible gaseous component. HF has also been described as a constituent of the volcanic ash and as contributing to environmental hazards (Cronin et al. 2003).

## Thenardite and phase III polymorph

Thenardite occurs associated with bloedite and picromerite around the main vent, and with halite at the smaller vent "vulcãozinho," while sodium sulphate (phase III) was identified in sample F19/17, along with thenardite and halite (Fig. 9), collected on the upper part of the pit walls with a temperature of 238 °C (Fig. 5c).

This sodium sulphate with five polymorphs has been found as precipitates around fumaroles elsewhere, e.g., in Tolbachik volcano (Pekov et al. 2014) and Kudriavy volcano, Kurile Islands (Wahrenberger et al. 2002) in Russia, and on the "Cueva Del Tigre" lava tube, Argentina (Benedetto et al. 1998). $Na_2SO_4$ exhibits a variety of phase transitions between its five anhydrous polymorphs (labeled I–V, according to Kracek 1929). The phase stability, transition temperatures, and structures have been studied by many authors (e.g., Mehrotra et al. 1975; Rasmussem et al. 1996; Vidya and Lakshminarasappa 2013; Taide et al. 2015) and the phase transformation sequence can be described as $V \leftrightarrow^{200°C} III \leftrightarrow^{230°C} II \leftrightarrow^{237°C} I \leftrightarrow^{883°C}$ melt. $Na_2SO_4$ forms two naturally occurring minerals: mirabilite ($Na_2SO_4.10H_2O$) and thenardite ($Na_2SO_4$). At room temperature, phase V (thenardite) is known to be stable while phase III is metastable. Phases I and II are high-temperature polymorphs, and phase II has a narrow stability zone. Phase IV is considered to be metastable (Taide et al. 2015). In the high-temperature polymorph, $Na_2SO_4$ (I), up to 30% cation vacancies can be generated by substitution of $Na^+$ by bi- and trivalent ions (Eysel et al. 1985). Recently, a new mineral, metathenardite [high-temperature hexagonal polymorph, $Na_2SO_4$ (I)], was approved by the International Mineralogical Association, Commission on New Minerals, Nomenclature and Classification (IMA 2015-102) as a dimorph of thenardite (Pekov et al. 2016). Choi and Lockwood (2005) found that phase III remains stable for more than 1 year at room

temperature in dried air, but in the normal atmosphere, phase III slowly reverts to phase V, while for Bobade et al. (2009) the transformation sequences of $Na_2SO_4$ while cooling (I → III → V) and heating (V → I) in ambient conditions are different.

To the best of our knowledge, this is the first time that thenardite and $Na_2SO_4$ (phase III) have been found simultaneously in incrustations. Fogo volcano has different atmospheric conditions from those previously used in the study of these minerals, due to the occurrence of summer rainfall at the beginning of autumn and only rare cloudbursts during the rest of the year, as well as low relative humidity (RH). These conditions allow the initial mineralogical phases to be conserved for a longer time before hydration or phase transition takes place. On the contrary, fumarole products from Vesuvius, some of them important due to their rarity, are subject to rapid alteration or, since they are quite soluble, are quickly carried off by rain shortly after their formation (Pelloux 1927).

The results of experiments, performed under various RH conditions, on sodium sulphate crystallization at room temperature (Rodriguez-Navarro et al. 2000), along with the arguments of Brodale and Giauque (1972) that although phase III is thermodynamically unstable at all temperatures it can exist indefinitely if kept dry, support our observations. In reality, the first authors studied the system $Na_2SO_4$-$H_2O$, namely the two phases considered stable at room temperature, thenardite and mirabilite. With high evaporation rate conditions (low RH), they observed the precipitation of thenardite directly from the saturated solution at temperatures below 32.4 °C (transition point of mirabilite-thenardite). At very low RH conditions (below 15%), occasionally they found crystals of thenardite (V) with a small amount of phase III (without formation of mirabilite), being the heterogeneous nucleation of thenardite in a supersaturated solution, the reason for its formation at temperatures below the transition point. Mirabilite was never found in incrustations from Fogo volcano; the low RH and high fast evaporation conditions explains the co-existence of $Na_2SO_4$ (V) and phase III in the same sample. These two phases are both metastable at 244 °C, and they are in equilibrium at that point, as shown by the free energy diagrams of Brodale and Giauque (1972); the stability of phase III at lower temperatures is possible for long times in a dry environment, being RH a key factor for that permanence as also shown by Linnow et al. (2006). Considering that thenardite has been used in many applications, such as for thermal energy storage (Vidya and Lakshminarasappa 2013), and that sodium sulphate is the most widely used salt in accelerated weathering tests of natural rocks and building materials (Rodriguez-Navarro et al. 2000; Steiger and Asmussen 2008), the present data are important to complement the previously recorded transition temperatures and phase stability laboratorial studies. The co-existence of these two polymorphs is proof that nature could produce what had been observed in strictly defined conditions in the laboratory (Linnow et al. 2006), as well as indicating that a high $Na_2SO_4$ supersaturated solution gave rise to the incrustations.

## Comparison with previous eruptions

Comparing the mineralogical phases identified in incrustations resulting from the 2014–2015 eruption of Fogo volcano with those found following the 1995 eruption (Figueiredo 1997; Figueiredo et al. 1997) shows that some minerals are common to both eruptions (sulfur, gypsum, anhydrite, halite, ralstonite). Others, however, were only identified in the 1995 event, namely alums, $MAl(SO_4)_2.12H_2O$, both sodic (M = Na) and potassic (M = K), halotrichite ($FeAl_2(SO_4)_4.22H_2O$), and sylvite (KCl)—only associated with halite and occasionally "soluble anhydrite" ($\gamma$-$CaSO_4$); natrojarosite ($NaFe_3(SO_4)_2(OH)_6$) was also identified in association with others minerals (Silva 1999), and an orange gel with minute, dispersed white grains (ralstonite). This amorphous, highly hygroscopic gel was heated to 600 °C, resulting in the loss of volatile constituents (mainly Cl and Tl) and in the formation of litharge (red PbO) together with a multiple oxide with bixbyite-type crystal structure (Figueiredo 1997).

Two distinct zones resulting from the 1995 eruption characterized the fumarole field (Silva 1999): one of high temperature (> 600 °C) with only white incrustations (mainly halite and more rarely sylvite), and another one with lower temperatures (between 85 °C and around 500 °C), in which the other minerals above mentioned were abundant. The observation of a zone in which there were only volcanic gases rich in chlorine raised the question as to whether there was an input of sea water into the magmatic chamber, although no studies were performed to investigate this hypothesis (Silva 1999); however, descriptions in Ribeiro (1998) relating to material of the 1785 Fogo eruption indicated the same idea. Halite and sylvite were not found associated with other minerals during the 1995 eruption of Fogo. This is contrary to the observations of other authors who found minerals as fumarole incrustations in silica-tubes (e.g., Stoiber and Rose 1974; Le Guern and Bernard 1982; Symonds et al. 1987; Quisefit et al. 1989; Toutain et al. 1990; Symonds et al. 1992), including the 2014–2015 sampling of Fogo (this work).

In addition to the above mentioned mineral species, sampling of the 1995 incrustation field, carried out in mullite tubes (Silva 1999), revealed anhydrite, steklite ($KAl(SO_4)_2$), and millosevichite ($Al_2(SO_4)_3$) in the lower part of the tubes (around 500 °C) and alunogen ($Al_2(SO_4)_3.16H_2O$) in the upper part. Conversely, the presence of alunogen (upper part of the tubes) and K-alum (field) along with Na-alum, halotrichite, and the orange gel suggests a high RH at the time of sampling (it rained around that time on the island), in apparent opposition to the observed anhydrous species.

The 2014–2015 eruption created a lower temperature fumarole field (< 250 °C), formed by incrustations of sulfur, halite, anhydrite, bassanite, gypsum, thenardite and its polymorph (phase III), tamarugite, picromerite, bloedite, bianchite, and ralstonite, minerals which are comparatively less hydrated than those identified for the previous eruptive event, probably due to lower RH and temperature. For instance, the dehydration of K-alum proceeds from crystalline $KAl(SO_4)_2.12H_2O$ to amorphous phases, and then to crystalline $KAl(SO_4)_2$ at around 240 °C (Kishimura et al. 2015). Conversely, Na-alum dehydrates directly to tamarugite without giving rise to the intermediate mendozite phase ($NaAl(SO_4)_2.11H_2O$) (Fang and Robinson 1972). The recognition of the unnamed phase, $NaAl(SO_4)_2$, in Santiaguito (Stoiber and Rose 1974) led us to suppose that tamarugite could result from the hydration of that phase instead of from a solution of sodium sulphate plus aluminum sulphate.

## Volcanic gas composition

Based on the mineralogy and chemistry data for the incrustations, Ca is the major cation present; the low temperature of fumaroles allied to the presence of fluorine gas (indicated by the occurrence of ralstonite) suggests its provenance from both degassing of Ca-rich magma and a possible wall-rock input (Africano and Bernard 2000). It is thought that the metals $Na^+$, $K^+$, $Mg^{2+}$, and $Ca^{2+}$ degas from the magma as chlorides (e.g., NaCl, KCl, $MgCl_2$, and $CaCl_2$) (Martin et al. 2010). The origin of sulphate aerosols was assumed to be the slow oxidation of gaseous $SO_2$, but studies by Allen et al. (2002) showed that these particles could be emitted directly from volcanic vents. $SO_2$, $H_2S$, $H_2$, $CO_2$, and $H_2O$ emission rates were measured before (Dionis et al. 2015a), and during the 2014–2015 eruption, representing the first $SO_2$ plume measurements ever carried out during an eruption of this volcano (Hernández et al. 2015): an increase in the $SO_2/H_2S$ ratio plus a decrease in $CO_2/SO_2$ was observed, which is indicative of the injection of $SO_2$-rich hot magmatic gases into the $H_2S$-rich hydrothermal system of Pico do Fogo volcano as reported by Hernández et al. (plume emissions: 10,688 t $day^{-1}$ of $CO_2$, 57 t $day^{-1}$ $H_2S$, 18 t $day^{-1}$ $H_2$, and 24,245 t $day^{-1}$ $H_2O$). However, the formation mechanism of gypsum can also include the action of sulfurous volcanic gases on Ca-bearing rocks (Deer et al. 1967).

Some authors (references in Dionis et al. 2015b) proposed four phases for the geological evolution of Fogo including the uplift of a seamount series composed of carbonatites and alkaline basalts, and recent studies classified the erupted magmas as alkaline, tephrites, and phonotephrites (Mata et al. 2017). The occurrence of carbonatite rocks is very rare in an oceanic setting; nevertheless, oceanic carbonatites have been reported at some islands of the Cape Verde archipelago (e.g., Assunção et al. 1965; Silva et al. 1981; Martins et al. 2010) and their origin has been linked to mantle plumes, composed of recycled oceanic crust plus carbonated sediments (Doucelance et al. 2010 and references herein).

## Toxic elements

From the elements identified in incrustations and altered rocks, some of them (e.g., As, Se, Tl, Pb) may raise environmental concerns due to their toxicity, which is dependent on various factors (Wu and Sun 2016). For example, the major inorganic forms of As include the trivalent arsenite and the pentavalent arsenate. Exposure to As occurs orally (ingestion), by inhalation or by skin contact. The toxic effects of As are highly influenced by its oxidation state and solubility, as well as many other intrinsic and extrinsic factors, for example inorganic $As^{3+}$ is 2–10 times more toxic than $As^{5+}$ (Tchounwou et al. 2012).

Conversely, Se is known for its toxicity (Lenz and Lens 2009), which develops via a complex cycle involving adsorption by soil components (clays and other particulate minerals) and subsequent incorporation into plants, where it can accumulate (Ellis and Salt 2003). In the natural environment, it occurs as an element ($Se^0$) with two allotropes, orthorhombic and monoclinic, as anions—selenide ($Se^{2-}$) and diselenide ($Se_2^{2-}$)—and as cations—selenite ($Se^{4+}$) and selenate ($Se^{6+}$). However, Se is also recognized as being an essential nutrient for animals, humans, and microorganisms. The occurrence of such elements is a major health hazard concern as local populations use sulfur and white materials as treatment for some human and animal diseases (by mixing and drinking with water for example). To clarify the speciation state of Se and the nature of Se-carrier phase(s) on incrustations samples, an X-ray absorption spectroscopy study (XANES) using synchrotron radiation has been undertaken at the Se *K*-edge (Silva et al. 2018). Different situations were observed: $Se^{6+}$ tetrahedral coordination, in a mixture of bassanite and anhydrite, due to the replacement of S by Se in $SO_4$ tetrahedra; $Se^{4+}$ pyramidal coordination in ralstonite, where selenium is probably linked to oxygen; and $Se^0$ in a sulfur sample due to diadochic replacement of S by Se.

## Conclusions

The fumarole incrustations resulting from the low temperature (< 250 °C) degassing of Fogo volcano are mainly composed of sulfur and sulphates, plus halides (fluoride and chloride). In the two last eruptions (1995 and 2014–2015), the mineral halite (NaCl) was identified in the higher temperature zone of the fumarole field, but in the more recent eruption it was associated with thenardite and a polymorph of $Na_2SO_4$ (phase III). To the best of our knowledge, this is the first time that

thenardite and its polymorph have been reported as co-existing in incrustations, probably due to the atmospheric conditions at Fogo volcano (summer rainfall at the beginning of autumn and only rare cloudbursts in the rest of the year creating low relative humidity) that are critical for the preservation and occurrence of these minerals. Also, this situation indicates that a high $Na_2SO_4$ supersaturated solution gave rise to the incrustations.

In addition to halite, thenardite, and $Na_2SO_4$ (III), sodium, magnesium, potassium, and calcium minerals were observed: tamarugite ($NaAl(SO_4)_2.6H_2O$), bloedite ($Na_2Mg(SO_4)_2.4H_2O$), ralstonite ($Na_xMg_xAl_{1-x}(F,OH)_3.(H_2O)n$), bianchite ($(Zn_{0.69}Fe_{0.21}Mg_{0.10})SO_4.6H_2O$), picromerite ($K_2Mg(SO_4)_2.6H_2O$), anhydrite ($CaSO_4$), bassanite ($CaSO_4.1/2H_2O$), and gypsum ($CaSO_4.2H_2O$). The same mineral groups were found in the 1995 eruption, but different species were observed, namely alums, $MAl(SO_4)_2.12H_2O$, both sodic (M = Na) and potassic (M = K), and sylvite (KCl), all of which have been described in fumarole incrustations at other volcanoes.

Calcium is the major cation present, suggesting that its provenance is from degassing of Ca-rich magma as indicated by the occurrence of carbonatites at some of the Cape Verde islands. F, Cl, and Br were also detected in the two events, as well as As and Se, plus the heavy metals Tl and Pb (potentially hazardous to health), which are indicative of the composition of the volcanic gases.

Contrasting with the formation of compounds/minerals under strictly defined conditions in the laboratory, active volcanoes produce fumarole incrustations that are an indirect source of information of the harmful elements exhaled, as well as a mineralogical finger print of these complex dynamic systems.

**Acknowledgments** This research received financial support from FCT (Fundação para a Ciência e Tecnologia) through project FIRE (PTDC/GEO-GEO/1123/2014). We acknowledge the European Synchrotron Radiation Facility for provision of synchrotron radiation facilities and in particular in using beamline BM 25A. Special thanks are due to the guides Manuel Montrond Fernandes (Izaquiel) and Edimar Montrond that helped us in the Fogo volcano. J.P. Veiga acknowledges funding by FEDER funds through the COMPETE 2020 Programme and National Funds through FCT-Portuguese Foundation for Science and Technology under the project UID/CTM/50025/2013 and the funding from the European Union Horizon 2020 research and innovation programme H2020-DRS-2015 GA nr. 700395 (HERACLES project). Carla Candeias would also like to acknowledge FCT by the grant SFRH/BPD/99636/2014 and UID/GEO/04035/2013. Special thanks are also due to Dr. Tonči Balić-Žunić, an anonymous reviewer and to the editors for their comments on the manuscript. We are also grateful to Dr. Lídia Quental for the satellite image of Fogo Island.

## References

Africano F, Bernard A (2000) Acid alteration in the fumarolic environment of Usu volcano, Hokkaido, Japan. J Volcanol Geotherm Res 97:475–495. https://doi.org/10.1016/S0377-0273(99)00162-6

Africano F, Van Rompaey G, Bernard A, Le Guern F (2002) Deposition of trace elements from high temperature gases of Satsuma-Iwojima volcano. Earth Planets Space 54:275–286. https://doi.org/10.1186/BF03353027

Aiuppa A (2015) Volcanic-gas monitoring. In: Schmidt A, Fristad KE, Elkins-Tanton LT (eds) Volcanism and Global Environmental Change. Cambridge University Press, pp 81–96. https://doi.org/10.1017/CBO9781107415683.009

Allen AG, Oppenheimer C, Ferm M, Baxter PJ, Horrocks LA, Galle B, McGonigle AJS, Duffell HJ (2002) Primary sulfate aerosol and associated emissions from Masaya volcano, Nicaragua. J Geophys Res 107:4682. https://doi.org/10.1029/2002JD002120

Assunção CFT, Machado F, Gomes RA (1965) On the occurrence of carbonatites in the Cape Verde Islands. Bol Soc Geol Port 16:179–188

Baker PE, Gass IG, Harris PG, Le Maitre RW (1964) The volcanological report of the Royal Society expedition to Tristan da Cunha, 1962. Philos Trans R Soc Lond A 256:439–575

Balić-Žunić T, Garavelli A, Jakobsson SP, Jonasson K, Katerinopoulos A, Kyriakopoulos K, Acquafredda P (2016) Fumarolic minerals: an overview of active European volcanoes. In: Nemeth K (ed) Updates in volcanology - from volcano modelling to volcano geology. InTech open access publishers, pp 267–322. https://doi.org/10.5772/64129

Benedetto C, Forti P, Galli E, Rossi A (1998) Chemical deposits in volcanic caves of Argentina. Int J Speleol 27B:155–162

Bobade SM, Gopalan P, Kulkarni AR (2009) Phase transition in $Na_2SO_4$: all five polymorphic transformations in DSC. Ionics 15:353–355. https://doi.org/10.1007/s11581-008-0272-6

Brodale GE, Giauque WE (1972) The relationship of crystalline forms I, III, IV, and V of anhydrous sodium sulfate as determined by the third law of thermodynamics. J Phys Chem 76:737–743. https://doi.org/10.1021/j100649a024

Carvalho MR, Mateus A, Nunes JC, Carvalho JM (2014) Origin and chemical nature of the thermal fluids at Caldeiras da Ribeira Grande (Fogo Volcano, S. Miguel Island, Azores). In: Sauer U, Dietrich P (Guest eds) Environ Earth Sci, Springer. https://doi.org/10.1007/s12665-014-3585-y

Chiodini G, Cioni R, Marini L, Panichi C (1995) Origin of the fumarolic fluids of Vulcano Island, Italy and implications for volcanic surveillance. Bull Volcanol 57:99–110. https://doi.org/10.1007/BF00301400

Chiodini G, Brombach T, Caliro S, Cardellini C (2002) Geochemical indicators of possible ongoing volcanic unrest at Nisyros Island (Greece). Geophys Res Lett 29:6–1-6-4. https://doi.org/10.1029/2001GL014355

Choi B-K, Lockwood DJ (2005) Peculiarities of the structural phase transitions in $Na_2SO_4$ (V): a Raman scattering study. J Phys Condens Matter 17:6095–6108. https://doi.org/10.1088/0953-8984/17/38/013

Cronin SJ, Neall VE, Lecointre JA, Hedley MJ, Loganathan P (2003) Environmental hazards of fuoride in volcanic ash: a case study from Ruapehu volcano, New Zealand. J Volcanol Geotherm Res 121:271–291. https://doi.org/10.1016/S0377-0273(02)00465-1

Day SJ, Heleno da Silva SIN, Fonseca JFBD (1999) A past giant lateral collapse and present-day flank instability of Fogo, Cape Verde Islands. J Volcanol Geotherm Res 94:191–218. https://doi.org/10.1016/S0377-0273(99)00103-1

De Moor JM, Fischer TP, Sharp ZD, King PL, Wilke M, Botcharnikov RE, Cottrell E, Zelenski M, Marty B, Klimm K, Rivard C, Ayalew D, Ramirez C, Kelley KA (2013) Sulfur degassing at Erta Ale (Ethiopia) and Masaya (Nicaragua) volcanoes: implications for degassing processes and oxygen fugacities of basaltic systems. Geochem Geophys Geosyst 14:4076–4108. https://doi.org/10.1002/ggge.20255

Deer WA, Howie RA, Zussman J (1967) Gypsum. In: Rock-forming minerals, non-silicates, vol 5. Longmans, London, pp 202–217

Dionis SM, Melián G, Rodríguez F, Hernández PA, Padrón E, Pérez NM, Barrancos J, Padilla G, Sumino H, Fernandes P, Bandomo Z, Silva S, Pereira JM, Semedo H (2015a) Diffuse volcanic gas emission and thermal energy release from the summit crater of Pico do Fogo, Cape Verde. Bull Volcanol 77:10. https://doi.org/10.1007/s00445-014-0897-4

Dionis SM, Pérez NM, Hernández PA, Melián G, Rodríguez F, Padrón E, Sumino H, Barrrancos J, Padilla GD, Fernandes P, Bandomo Z, Silva S, Pereira JM, Semedo H, Cabral J (2015b) Diffuse $CO_2$ degassing and volcanic activity at Cape Verde islands, West Africa. Earth Planets Space 67:48. https://doi.org/10.1186/s40623-015-0219-x

Doucelance R, Hammouda T, Moreira M, Martins JC (2010) Geochemical constraints on depth of origin of oceanic carbonatites: the Cape Verde case. Geochim Cosmochim Acta 74:7261–7282. https://doi.org/10.1016/j.gca.2010.09.024

Ellis DR, Salt DE (2003) Plants, selenium and human health. Curr Opin Plant Biol 6:273–279. https://doi.org/10.1016/S1369-5266(03)00030-X

Eysel W, Höfer HH, Keester KL, Hahn T (1985) Crystal chemistry and structure of $Na_2SO_4$ (I) and its solid solutions. Acta Crystallogr B 41:5–11

Fang JH, Robinson PD (1972) Crystal structures and mineral chemistry of double-salt hydrates: II. The crystal structure of mendozite, $NaAl(SO_4)_2.11H_2O$. Am Min 57:1081–1088

Ferrara G, Garavelli A, Pinarelli L, Vurro F (1995) Lead isotope composition of the sublimates from the fumaroles of Vulcano (Aeolian Islands, Italy): inferences on the deep fluid circulation. Bull Volcanol 56:621–625. https://doi.org/10.1007/BF00301466

Figueiredo MO (1997) Orange gel masses associated with the eruption of 1995 on Fogo Island: a new mineral? (in Portuguese). In: Réffega A et al (eds) A erupção vulcânica de 1995 na ilha do Fogo, Cabo Verde, IICT, Lisbon, Portugal, pp 201–210

Figueiredo MO, Silva LC, Pereira da Silva T, Torres PC, Mendes MH (1997) Mineralogy of the incrustations resulting from the fumarole activity from the 1995 eruption of the Fogo island, Cape Verde (in Portuguese). In: Réffega A et al (eds) A erupção vulcânica de 1995 na ilha do Fogo, Cabo Verde, IICT, Lisbon, Portugal, pp 187–199

Figueiredo MO, Silva TP, Basto MJ, Ramos MT, Chevallier P (1999) Indirect monitoring of heavy metals in volcanic gases by synchrotron X-ray microprobe (μ-SRXRF) qualitative analysis of sublimates. J Anal At Spectrom 14:505–507. https://doi.org/10.1039/A808103D

Figueiredo E, Fonte J, Lima A, Veiga JP, Silva RJC, Mirão J (2018) Ancient tin production: slags from the Iron age Carvalhelhos hillfort (NW Iberian Peninsula). J Archaeol Sci 93:1–16. https://doi.org/10.1016/j.jas.2018.02.007

Fischer TP (2008) Fluxes of volatiles ($H_2O$, $CO_2$, $N_2$, Cl, F) from arc volcanoes. Geochem J 42:21–38. https://doi.org/10.2343/geochemj.42.21

Flörke OW (1952) Kristallographische und röntgenographische Untersuchungen im System, $CaSO_4$-$CaSO_4.2H_2O$. Neues Jahrb Min, Abh 84:189–240

Giggenbach WF (1996) Chemical composition of volcanic gases. In: Scarpa R, Tilling RI (eds) Monitoring and mitigation of volcano hazards. Springer, Berlin, pp 221–256. https://doi.org/10.1007/978-3-642-80087-0_7

Global Volcanism Program (2017) Report on Fogo (Cape Verde). In: Venzke E (ed) Bulletin of the global volcanism network 42:9. Smithsonian Institution

Le Guern F, Bernard A (1982) Etude des mecanismes de condensation des gaz magmatiques - exemple de l'Etna (Italie). Bull Volcanol 45:161–166. https://doi.org/10.1007/BF02597725

Hardie LA (1967) The gypsum-anhydrite equilibrium at one atmosphere pressure. Am Miner 52:171–200

Hernández PA, Melián GV, Dionis S, Barrancos J, Padilla G, Padrón E, Silva S, Fernandes P, Cardoso N, Pérez NM, Rodríguez F, Asensio-Ramos M, Calvo D, Semedo H, Alfama V (2015) Chemical composition of volcanic gases emitted during the 2014-15 Fogo eruption, Cape Verde. Geophys Res Abstr 17:EGU2015–EGU9577

Jakobsson SP, Leonardsen ES, Balic-Zunic T, Jónsson SS (2008) Encrustations from three recent volcanic eruptions in Iceland: the 1963-1967 Surtsey, the 1973 Eldfelland and the 1991 Hekla eruptions. Fjölrit Náttúrufræðistofnunar 52:65

Jenkins SF, Day SJ, Faria BE, Fonseca JFBD (2017) Damage from lava flows: insights from the 2014-2015 eruption of Fogo, Cape Verde. J Appl Volcanol 6:6. https://doi.org/10.1186/s13617-017-0057-6

Kishimura H, Imasu Y, Matsumoto H (2015) Thermal dehydration of potash alum studied by Raman spectroscopy and X-ray diffraction analysis. Mater Chem Phys 149-150:99–104. https://doi.org/10.1016/j.matchemphys.2014.09.049

Kodosky L, Keskinen M (1990) Fumarole distribution, morphology, and encrustation mineralogy associated with the 1986 eruptive deposits of Mount St. Augustine, Alaska. Bull Volcanol 52:175–185. https://doi.org/10.1007/BF00334803

Kracek FC (1929) The polymorphism of sodium sulphate. I: thermal analysis. J Phys Chem 33:1281–1303. https://doi.org/10.1021/j150303a001

Lacroix A (1907) Les mineraux des fumerolles de l'eruption du Vesuve en avril 1906. Bull Soc Min Fr 30:219–226

Lenz M, Lens PNL (2009) The essential toxin: the changing perception of selenium in environmental sciences. Sci Total Environ 407:3620–3633. https://doi.org/10.1016/j.scitotenv.2008.07.056

Linnow K, Zeunert A, Steiger M (2006) Investigation of sodium sulfate phase transitions in a porous material using humidity- and temperature-controlled X-ray diffraction. Anal Chem 78:4683–4689. https://doi.org/10.1021/ac0603936

Lombardi G, Sposato A (1981) Tamarugite from Vulcano, Aeolian Islands, Italy. Can Mineral 19:403–407

Maccaferri F, Richter N, Walter TR (2017) The effect of giant lateral collapses on magma pathways and the location of volcanism. Nat Commun 8:1097. https://doi.org/10.1038/s41467-017-01256-2

Mackenzie KM, Rodgers KA, Browne PRL (1995) Tamarugire, $NaAl(SO_4)_2.6H_2O$, from Te Kopia, New Zealand. Min Mag 59:754–757

Martin RS, Sawyer GM, Spampinato L, Salerno GG, Ramirez C, Ilyinskaya E, Witt MLI, Mather TA, Watson IM, Phillips JC, Oppenheimer C (2010) A total volatile inventory for Masaya volcano, Nicaragua. J Geophys Res 115:B09215. https://doi.org/10.1029/2010JB007480

Martins S, Mata J, Munhá J, Mendes MH, Maerschalk C, Caldeira R, Mattielli N (2010) Chemical and mineralogical evidence of the occurrence of mantle metasomatism by carbonate-rich melts in an oceanic environment (Santiago Island, Cape Verde). Mineral Petrol 99:43–65. https://doi.org/10.1007/s00710-009-0078-x

Mata J, Martins S, Mattielli N, Madeira J, Faria B, Ramalho RS, Silva P, Moreira M, Caldeira R, Moreira M, Rodrigues J, Martins L (2017) The 2014-15 eruption and the short-term geochemical evolution of the Fogo volcano (Cape Verde): evidence for small-scale mantle heterogeneity. Lithos 288-289:91–107. https://doi.org/10.1016/j.lithos.2017.07.001

Mehrotra BN, Hahn T, Arnold H, Eysel W (1975) Polymorphism of $Na_2SO_4$. Acta Crystallogr A 31(Supplement):S79

Melián G, Tassi F, Pérez N, Hernández P, Sortino F, Vaselli O, Padrón E, Nolasco D, Barrancos J, Padilla G, Rodríguez F, Dionis S, Calvo D, Notsu K, Sumino H (2012) A magmatic source for fumaroles and diffuse degassing from the summit crater of Teide volcano (Tenerife, Canary Islands): a geochemical evidence for the 2004–2005 seismic–volcanic crisis. Bull Volcanol 74:1465–1483. https://doi.org/10.1007/s00445-012-0613-1

Naughton JJ, Greenberg VA, Goguel R (1976) Incrustations and fumarolic condensates at Kilauea volcano, Hawaii: field, drill-hole and laboratory observations. J Volcanol Geotherm Res 1:149–165. https://doi.org/10.1016/0377-0273(76)90004-4

Orlando V, Franco T, Dario T, Robert PJ, Antonio C (2011) Submarine and inland gas discharges from the Campi Flegrei (southern Italy) and the Pozzuoli Bay: geochemical clues for a common hydrothermal-magmatic source. Procedia Earth Planet Sci 4:57–73. https://doi.org/10.1016/j.proeps.2011.11.007

Óskarsson N (1981) The chemistry of icelandic lava incrustations and the latest stages of degassing. J Volcanol Geotherm Res 10:93–111. https://doi.org/10.1016/0377-0273(81)90057-3

Óskarsson N (1984) Monitoring of fumarole discharge during the 1975–1982 rifting in Krafla volcanic center, North Iceland. J Volcanol Geotherm Res 22:97–121. https://doi.org/10.1016/0377-0273(84)90036-2

Palache C, Berman H, Frondel C (1951) The system of mineralogy. Wiley, London

Paonita A, Federico C, Bonfanti P, Capasso G, Inguaggiato S, Italiano F, Madonia P, Pecoraino G, Sortino F (2013) The episodic and abrupt geochemical changes at La Fossa fumaroles (Vulcano Island, Italy) and related constraints on the dynamics, structure, and compositions of the magmatic system. Geochim Cosmochim Acta 120:158–178. https://doi.org/10.1016/j.gca.2013.06.015

Pekov IV, Zubkova NV, Yapaskurt VO, Belakovskiy DI, Lykova IS, Vigasina MF, Sidorov EG, Pushcharovsky DY (2014) New arsenate minerals from the Arsenatnaya fumarole, Tolbachik volcano, Kamchatka, Russia. I. Yurmarinite, $Na_7(Fe^{3+},Mg,Cu)_4(AsO_4)_6$. Min Mag 78:905–917. https://doi.org/10.1180/minmag.2014.078.4.10

Pekov IV, Gurzhiy VV, Zubkova NV, Agakhanov AA, Belakovskiy DI, Vigasina MF, Sidorov EG (2016) Metathénardite, IMA 2015-102. CNMNC newsletter no. 30, April 2016, page 408. Min Mag 80: 407–413. https://doi.org/10.1180/minmag.2016.080.081

Pelloux A (1927) The minerals of Vesuvius. Am Miner 12:14–21

Prasad PSR, Ravikumar N, Krishnamurthy ASR, Sarma LP (1998) Role of impurities in gypsum-bassanite phase transition: a comparative Raman study. Curr Sci 75:1410–1414

Quisefit JP, Toutain JP, Bergametti G, Javoy M, Cheynet B, Person A (1989) Evolution versus cooling of gaseous volcanic emissions from Momotombo volcano, Nicaragua: thermochemical model and observations. Geochim Cosmochim Acta 53:2591–2608. https://doi.org/10.1016/0016-7037(89)90131-2

Rasmussem SE, Jørgensen J-E, Lundtoft B (1996) Structures and phase transitions of $Na_2SO_4$. J Appl Crystallogr 29:42–47. https://doi.org/10.1107/S0021889895008818

Ribeiro O (1998) The Fogo Island and its eruptions (in Portuguese). Comissão Nacional para as Comemorações dos Descobrimentos Portugueses, Lisbon

Richter N, Favalli M, Dalfsen EZ, Fornaciai A, Fernandes RMS, Pérez NM, Levy J, Victória SS, Walter TR (2016) Lava flow hazard at Fogo volcano, Cabo Verde, before and after the 2014-2015 eruption. Nat Hazards Earth Syst Sci 16:1925–1951. https://doi.org/10.5194/nhess-16-1925-2016

Rodríguez-Mercado JJ, Altamirano-Lozano M (2013) Genetic toxicology of thallium: a review. Drug Chem Toxicol 36:369–383. https://doi.org/10.3109/01480545.2012.710633

Rodriguez-Navarro C, Doehnea E, Sebastian E (2000) How does sodium sulfate crystallize? Implications for the decay and testing of building materials. Cem Concr Res 30:1527–1534

Rose WI (1973) Pattern and mechanism of volcanic activity at the Santiaguito volcanic dome, Guatemala. Bull Volcanol 37:73–94. https://doi.org/10.1007/BF02596881

Rosenberg PE (1988) Aluminum fluoride hydrates, volcanogenic salts from mount Erebus, Antarctica. Am Miner 73:855–860

Shinohara H (2013) Volatile flux from subduction zone volcanoes: insights from a detailed evaluation of the fluxes from volcanoes in Japan. J Volcanol Geotherm Res 268:46–63. https://doi.org/10.1016/j.jvolgeores.2013.10.007

Silva TP (1999) Minerochemistry of incrustations and fumarole sublimates from Fogo island volcano (Cape Verde) (in Portuguese). Dissertation equivalent to PhD, IICT-Instituto de Investigação Científica Tropical (ed), Lisbon, Portugal, 159 pp

Silva LC, Le Bas MJ, Robertson AHF (1981) An oceanic carbonatite volcano on Santiago, Cape Verde Islands. Nature 294:644–645. https://doi.org/10.1038/294644a0

Silva LC, Mendes MH, Torres PC, Palácios T, Munhá JM (1997) Petrography and mineralogy of the volcanic formations from the 1995 eruption of the Fogo island, Cape Verde (in Portuguese). In: Réffega A et al. (eds) A erupção vulcânica de 1995 na ilha do Fogo, Cabo Verde, IICT, Lisbon, Portugal, pp 165–170

Silva TP, de Oliveira D, Veiga JP, Ávila P, Candeias C, Salas-Colera E, Caldeira R (2018) Selenium retained by minerals from volcanic fumaroles at Fogo island (Cape Verde). In: Oliveira A et al (eds) Abstracts book of XIV Congresso de Geoquímica dos Países de Língua Portuguesa, UTAD, Portugal, pp 511–514

Solé VA, Papillon E, Cotte M, Walter P, Susini J (2007) A multiplatform code for the analysis of energy-dispersive X-ray fluorescence spectra. Spectrochim Acta 62:63–68. https://doi.org/10.1016/j.sab.2006.12.002

Steiger M, Asmussen S (2008) Crystallization of sodium sulfate phases in porous materials: the phase diagram $Na_2SO_4$–$H_2O$ and the generation of stress. Geochim Cosmochim Acta 72:4291–4306. https://doi.org/10.1016/j.gca.2008.05.053

Stoiber RE, Rose WI (1969) Recent volcanic and fumarolic activity at Santiaguito volcano, Guatemala. Bull Volcanol 33:475–502. https://doi.org/10.1007/BF02596520

Stoiber RE, Rose WI (1970) The geochemistry of central American volcanic gas condensates. GSA Bull 81:2891–2912. https://doi.org/10.1130/0016-7606(1970)81[2891:TGOCAV]2.0.CO;2

Stoiber RE, Rose WI (1974) Fumarole incrustations at active central American volcanoes. Geochim Cosmochim Acta 38:495–516. https://doi.org/10.1016/0016-7037(74)90037-4

Symonds RB, Rose WI, Reed MH, Lichte FE, Finnegan DL (1987) Volatilization, transport and sublimation of metallic and non-metallic elements in high temperature gases at Merapi volcano, Indonesia. Geochim Cosmochim Acta 51:2083–2101. https://doi.org/10.1016/0016-7037(87)90258-4

Symonds RB, Reed MH, Rose WI (1992) Origin, speciation, and fluxes of trace-element gases at Augustine volcano, Alaska: insights into magma degassing and fumarolic processes. Geochim Cosmochim Acta 56:633–657. https://doi.org/10.1016/0016-7037(92)90087-Y

Symonds RB, Rose WI, Bluth GJS, Gerlach TM (1994) Volcanic gas studies: methods, results, and applications. In: Carroll MR, Holloway JR (eds) Volatiles in Magmas. Reviews in Mineralogy, vol 30, pp 1–66 http://www.minsocam.org/MSA/RIM/Rim30.html

Taide ST, Ingle NB, Omanwar SK (2015) Characterization and photoluminescence studies of $Dy^{3+}$ doped $Na_2SO_4$ phosphor prepared by re-crystallization method. IOSR. J Appl Phys 7:27–32. https://doi.org/10.9790/4861-07312732

Taran Y, Zelenski M (2015) Systematics of water isotopic composition and chlorine content in arc-volcanic gases. Geol Soc Lond, Spec Publ 410(1):237–262. https://doi.org/10.1144/SP410.5

Tchounwou PB, Yedjou CG, Patlolla AK, Sutton DJ (2012) Heavy metal toxicity and the environment. In: Luch A (ed) Molecular, clinical and environmental toxicology. Exp Suppl 101. Springer, Basel, pp 133–164. https://doi.org/10.1007/978-3-7643-8340-4_6

Torres PC, Silva LC, Mota Gomes A (1995) Geology and volcanology of the 1995 eruption on the Fogo island-Cape Verde archipelago (in Portuguese). In: Porto University (ed) Memórias do Museu e

Laboratório Mineralógico e Geológico da Faculdade de Ciências da Universidade do Porto, pp 1019–1023

Torres PC, Madeira J, Silva LC, Silveira AB, Serralheiro A, Mota Gomes, A (1997) Geologic map of the historical eruptions of Fogo Island: review and update (in Portuguese). In: Réffega A et al (eds) A erupção vulcânica de 1995 na ilha do Fogo, Cabo Verde, IICT, Lisbon, Portugal, pp 119–132

Toutain JP, Aloupogiannis P, Delorme H, Person A, Blanc P, Robaye G (1990) Vapor deposition of trace elements from degassed basaltic lava, piton de la Fournaise volcano, Reunion Island. J Volcanol Geotherm Res 40:257–268. https://doi.org/10.1016/0377-0273(90)90124-X

Vergasova LP, Filatov SK (2016) A study of volcanogenic exhalation mineralization. J Volcanol Seismol 10:71–85. https://doi.org/10.1134/S0742046316020068

Vidya YS, Lakshminarasappa BN (2013) Preparation, Characterization, and Luminescence Properties of Orthorhombic Sodium Sulphate. Phys Res Int 2013:641631, 7 pages. https://doi.org/10.1155/2013/641631

Vieira G, Pina P, Mora C, Fernandes R, Almeida P, Dumont S, Martins B, Candeias C, Oliveira C, Ramalho RS (2017) Very high-resolution aerophotogrametric survey of the 2014/2015 lava flow field of Fogo volcano (Cape Verde). Proceedings of the 5th International Conference on "Small Unmanned Aerial Systems for Environmental Research", Vila Real, Portugal, pp 49–50

Wahrenberger C, Seward TM, Dietrich V (2002) Volatile trace-element transport in high-temperature gases from Kudriavy volcano (Iturup, Kurile Islands, Russia). In: Hellmann R, Wood SA (eds) Water-rock interactions, ore deposits, and environmental geochemistry: a tribute to David A. Crera. Geochem Soc Spec Publ 7:307–327. https://ci.nii.ac.jp/naid/10018296233

Williams SN, Self S (1983) The October 1902 Plinian eruption of Santa Maria volcano, Guatemala. J Volcanol Geotherm Res 16:33–56. https://doi.org/10.1016/0377-0273(83)90083-5

Wu D, Sun S (2016) Speciation analysis of As, Sb and Se. Trends Env Anal Chem 11:9–22. https://doi.org/10.1016/j.teac.2016.05.001

Zelenski M, Taran Y (2011) Geochemistry of volcanic and hydrothermal gases of Mutnovsky volcano, Kamchatka: evidence for mantle, slab and atmosphere contributions to fluids of a typical arc volcano. Bull Volcanol 73:373–394. https://doi.org/10.1007/s00445-011-0449-0